

# A rare-earth-ion-doped waveguide based on a standard photonics technology for quantum signal processing

N. Sinclair,<sup>1</sup> D. Oblak,<sup>1</sup> C. W. Thiel,<sup>2</sup> R. L. Cone,<sup>2</sup> and W. Tittel<sup>1</sup>

<sup>1</sup>*Institute for Quantum Science and Technology, and Department of Physics & Astronomy,  
University of Calgary, Calgary, Alberta T2N 1N4, Canada*

<sup>2</sup>*Department of Physics, Montana State University, Bozeman, Montana 59717, USA*

We measure properties of the 795 nm  $^3\text{H}_6$  to  $^3\text{H}_4$  transition of a rare-earth-ion-doped waveguide,  $\text{Tm}^{3+}:\text{Ti}^{4+}:\text{LiNbO}_3$ , at temperatures as low as 800 mK. Coherence and hyperfine population lifetimes up to 117  $\mu\text{s}$  and 2.5 hours, respectively, are observed. They are at least one order of magnitude greater than those measured at 3 K, and match those observed in a bulk  $\text{Tm}^{3+}:\text{LiNbO}_3$  crystal under similar conditions. Furthermore, taking advantage of these properties, we prepare a 0.5 GHz-bandwidth atomic frequency comb quantum memory of finesse  $>2$  on a vanishing background. Finally, we measure high Rabi frequencies and calculate a transition dipole moment of  $\sim 10^{-32}$  C·m, which is equivalent to that of  $\text{Tm}^{3+}:\text{LiNbO}_3$ . Our results show the suitability of rare-earth-doped waveguides created using industry-standard Ti-indiffusion in  $\text{LiNbO}_3$  for on-chip quantum applications.

PACS numbers: 42.50.Md, 42.82.Gw, 42.50.Gy, 32.70.Cs

Integrated optics offers the possibility of scalable manipulation of light due to small guiding volume and chip size, ever-improving fabrication methods, and low loss [1, 2]. These attractive features have also enabled advanced experiments and applications of quantum optics and quantum information processing, with many demonstrations using telecommunication-industry-standard Ti-indiffused  $\text{LiNbO}_3$  waveguides, see e.g. [3–9] and references therein. Moreover, the ability to combine many components onto a single substrate is required for the implementation of an integrated quantum information processing node that performs local operations, interconnects, and measurements for quantum-secured computing and communications [10]. For example, a chip containing multiplexed sources of entangled photon pairs, Bell-state analyzers, photon number-resolving nondestructive photon detection, and feed-forward qubit-mode translation and selection, e.g. using frequency shifts or on-demand quantum memories, could pave the way to the development of a practical quantum repeater [9, 11, 12]. A promising avenue to this end, and to quantum information processing in general, is based on qubit interfaces using rare-earth-ion-doped (REI-doped) crystals at cryogenic temperatures [3, 5, 12–16]. Thus, the development of rare-earth-ion-doped waveguide crystals constitutes an exciting and important path towards applications.

Many ground-breaking quantum optics experiments, in particular quantum memory for light [13–16], are based on cryogenically cooled REIs doped into a variety of bulk crystals. However, work employing REI-doped crystalline waveguides has, until only the past year, been restricted to  $\text{LiNbO}_3$  – generally doped with thulium – into which waveguides were fabricated by means of titanium indiffusion [3, 5, 9, 12, 17]. A likely explanation for the lack of investigations using other REIs in  $\text{Ti}^{4+}:\text{LiNbO}_3$  is that an earlier low-temperature charac-

terization of  $\text{Tm}^{3+}:\text{Ti}^{4+}:\text{LiNbO}_3$ , which was performed at 3 K, revealed non-ideal properties for quantum signal processing [18]. Specifically, optical coherence and hyperfine-level lifetimes were shown to be significantly reduced compared to those of a bulk  $\text{Tm}^{3+}:\text{LiNbO}_3$  crystal at the same temperature [19], possibly due to perturbations stemming from the introduction of Ti. As alternatives, several groups have recently explored the use of  $\text{Y}_2\text{SiO}_5$  crystals together with evanescent wave-mediated planar waveguides [20], ion beam-milled photonic crystals [21], or waveguides created via femtosecond laser writing [22] – all of which guide light in unperturbed regions of the REI-doped crystal. While the results are promising, it is generally still unclear how a waveguide fabrication process affects all relevant REI properties for quantum applications and, being the topic of our study, if good properties can be retained using industry-standard Ti-indiffusion in  $\text{LiNbO}_3$ .

To investigate this question, we measure optical properties of the  $^3\text{H}_6$  to  $^3\text{H}_4$  transition of  $\text{Tm}^{3+}:\text{Ti}^{4+}:\text{LiNbO}_3$  using photon echoes and spectral hole burning [23] at temperatures as low as 800 mK and with applied magnetic fields up to 600 Gauss. We find at least one order of magnitude improvement of critical properties (optical coherence and hyperfine population lifetimes) compared to those measured previously at 3 K [18]. Moreover, the measured properties match those observed using  $\text{Tm}^{3+}:\text{LiNbO}_3$  bulk crystals under similar conditions [24], and improve upon those observed with other REI-doped waveguides [20–22]. In addition, our measurements establish a ratio of coherence lifetime to ( $^3\text{H}_4$ ) excited-state population lifetime that is greater than one [18, 25], which benefits applications in the field of cavity quantum electrodynamics [26] or employing cross-phase modulation [12]. To show key requirements for efficient quantum information processing, we burn per-

sistent holes to transparency, and tailor a 0.5 GHz-bandwidth atomic frequency comb (AFC) [14, 15] with a finesse of three on a vanishing absorption background. Finally, we measure Rabi frequencies that allow the calculation of a bulk-equivalent [19] transition dipole moment of  $\sim 10^{-32}$  C·m. This establishes that waveguide fabrication does not reduce the dipole moment – an important finding in view of achieving large light-matter coupling.

*Experimental methods*—Measurements are carried out using a 15.7 mm-long  $\text{Ti}^{4+}:\text{Tm}^{3+}:\text{LiNbO}_3$  waveguide. It is created by increasing the index of refraction of a  $\sim 4$   $\mu\text{m}$ -wide strip through indiffusion of Ti into the surface of a 0.9 mm-thick, 0.7% Tm-indiffusion-doped lithium niobate wafer [18]. The wafer is mounted inside a pulse tube cryocooler on a Cu stage attached to a GGG salt pellet that generates temperatures as low as 800 mK (measured near the crystal) via adiabatic demagnetization. Light is directed into, and out of, the waveguide using single-mode fiber butt-coupling. Transmission through the entire cryogenic setup is 10-20%, mainly limited by imperfect overlap between fiber and waveguide modes as well as reflections from the uncoated surfaces. Magnetic fields of up to 2 T are applied parallel to the crystal's c-axis using a superconducting solenoid coil. We employ an external-cavity diode laser, producing polarized light set normal to the crystal's c-axis [18, 19]. Its wavelength is tuned between 795.5 and 799.0 nm (vac.) using a diffraction grating. These wavelengths are chosen to ensure the optical depth of the crystal is no more than approximately 1.4. A 400 MHz acousto-optic modulator is employed to produce pulses as short as 50 ns for photon echo measurements, or as long as several ms for hole burning and spectral tailoring. Spectral features are probed by ramping the laser frequency using a  $\text{LiNbO}_3$  waveguide phase modulator driven with a sawtooth-modulated voltage [5, 9]. Optical transmission is detected using a 1 GHz (2 MHz) AC (DC)-coupled amplified diode, digitized by an oscilloscope. To minimize errors due to laser power fluctuations, jitter, and noise we average over many repetitions of the same experiment. Furthermore, in cases where it is undesired, persistent spectral hole burning is mitigated by slowly sweeping the laser frequency.

*Results*—Long optical coherence lifetimes are a key reason why rare-earth-ion-doped crystals are employed for quantum applications [14–16]. Using a two-pulse photon echo decay, we measure the coherence lifetime  $T_2$  of the transition at 795.6 nm in a 300 G magnetic field, at a temperature of 810 mK, and with a laser peak power inside the waveguide of  $\sim 0.4$  mW (set to minimize excitation-induced decoherence (EID) [28] while simultaneously ensuring the echo intensity is above the noise level). The decay, as shown in Fig. 1, is fitted using

$$I(t_{12}) = I_0 e^{-2\left(\frac{t_{12}}{T_2}\right)^x}, \quad (1)$$

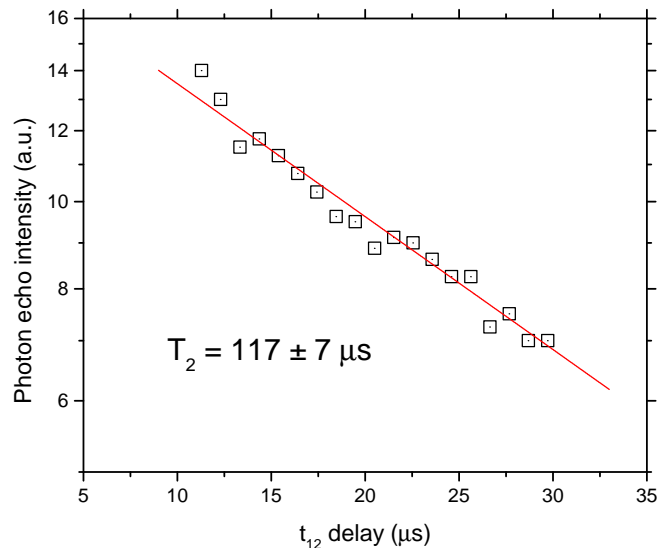


FIG. 1: Two pulse photon echo decay. Measurements at a wavelength of 795.6 nm, using 300 G magnetic field, and at a temperature of 810 mK yield a coherence lifetime of 117  $\mu\text{s}$ . The decay is exponential and does not exhibit any time-dependent increase of decoherence i.e.  $x = 1$  in Eq. 1.

where  $t_{12}$  is the delay between the two excitation pulses,  $I_0$  is the echo intensity at  $t_{12} = 0$ , and  $x$  describes the decay shape [29]. We find a coherence lifetime of 117  $\mu\text{s}$ ; 70 times greater than what we measured in  $\text{Tm}^{3+}:\text{Ti}^{4+}:\text{LiNbO}_3$  at 3.5 K [18], and larger than the 86  $\mu\text{s}$  we observed using a  $\text{Tm}^{3+}:\text{LiNbO}_3$  bulk crystal at 790 mK temperature, 794.25 nm wavelength, and  $\sim 150$  Gauss magnetic field [24]. We note that temperature-dependent measurements of  $T_2$  indicate a factor of three larger direct phonon-coupling rate in the waveguide as compared to that measured in the bulk [25]. We expect that  $T_2$  can be increased further by probing ions that absorb at wavelengths towards the center of the inhomogeneous line, as these ions are more characteristic of typical crystal environments than the ions currently probed. We note that the larger  $T_2$  of the waveguide in comparison to that measured in the corresponding bulk crystal under similar conditions was not expected. This difference may be due to EID during the bulk crystal  $T_2$  measurement, however, more experiments are needed to verify this explanation.

In conjunction with a sufficiently-long  $T_2$ , many quantum applications require the ability to spectrally tailor the absorption profile of a rare-earth-ion transition. This requires long-lived sub-levels to optically pump ions, e.g. to create transparency or efficient memories. Therefore, we measure the dynamics of the Tm hyperfine sub-levels under 600 G field, at a temperature of 850 mK, and at a wavelength of 795.5 nm using time-resolved persistent spectral hole burning. Under application of an external

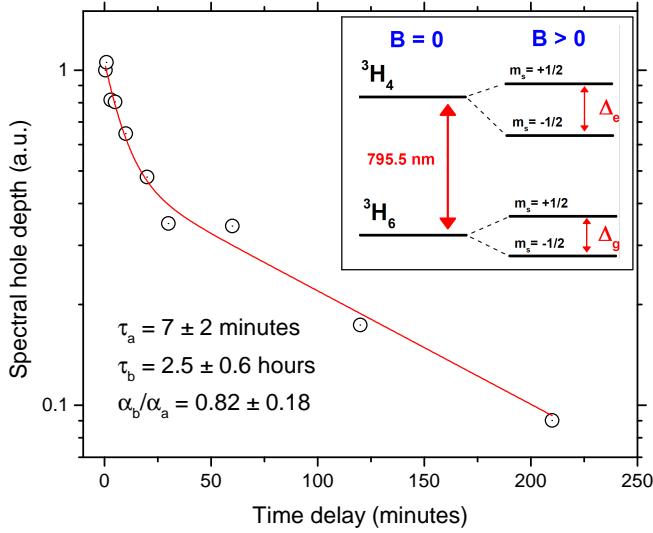


FIG. 2: Persistent spectral hole burning decay. Measurements at a wavelength of 795.5 nm, under a magnetic field of 600 G, and at a temperature of 850 mK yield a population decay that follows a double exponential. Inset: Simplified energy level diagram (not to scale) showing optically excited levels and hyperfine levels split by the applied magnetic field.

magnetic field, sub-levels arise due to an enhanced effective nuclear Zeeman effect from the hyperfine coupling of the  $^{169}\text{Tm}$  spin-1/2 nucleus to the electronic states [23]. This splits both the excited and ground states into pairs ( $m_s = \pm 1/2$ ) with a difference in energy splitting of  $|\Delta_e - \Delta_g| \sim 140 \text{ kHz/G}$  [19, 25], allowing optical pumping of the nuclear spin populations between hyperfine states. The resultant spectral hole in the optical absorption decays as the nuclear spin population returns to thermal equilibrium as is shown in Fig. 2, with a simplified sub-level structure depicted in the inset. We fit the decay using a double exponential,

$$\Delta\alpha(t_d) = \Delta\alpha_a e^{-t_d/\tau_a} + \Delta\alpha_b e^{-t_d/\tau_b}, \quad (2)$$

where  $t_d$  is the time delay between hole burning and probing,  $\tau_a$  and  $\tau_b$  are two different hole lifetimes, and  $\Delta\alpha_a$  and  $\Delta\alpha_b$  are the relative amplitudes of the two population components present in the hole decay. We find two exponentials, similar to what we measured in this material at 3.5 K [18], except now with lifetimes of 7 minutes, and 2.5 hours. These lifetimes are two orders of magnitude greater than those measured at 3.5 K [18], and agree well with those measured using a  $\text{Tm}^{3+}:\text{LiNbO}_3$  bulk crystal under similar conditions [24]. Indeed, reduction in phonon scattering at lower temperatures predicts an increase in population lifetimes of hyperfine levels. Although we have not yet investigated the origin of the double decay, we conjecture that two components may arise from inequivalent  $\text{Tm}^{3+}$  sites in the lattice or possibly from a combination of optical pumping of the

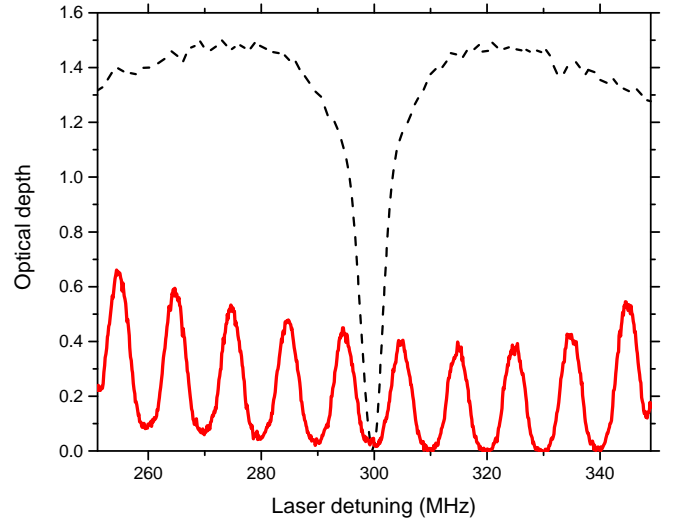


FIG. 3: A spectral hole (dashed curve) and AFC (solid curve) created under 500 G and 2 kG magnetic fields, respectively, at a temperature of 800 mK and a wavelength of 795.5 nm.

lithium and niobium spins through the superhyperfine interaction in addition to pumping of the  $\text{Tm}^{3+}$  nuclear spin states [19, 25]. The double decay at this temperature seems to be intrinsic of the material and not a result of waveguide fabrication since a similar behavior is also observed in the bulk crystal [24].

We also demonstrate that our Tm-doped waveguide may be used for efficient quantum applications. Going beyond what we have shown at 3 K, and what has been shown with other rare-earth-ion-doped waveguides, we take advantage of the hyperfine sub-level properties to generate a persistent spectral hole on a vanishing absorption background as shown in Fig. 3. Specifically, at a temperature of 800 mK, wavelength of 795.5 nm, and using a 500 G magnetic field, we burn a spectral hole during several ms, wait for 100 ms, and then, with reduced laser power, sweep the laser frequency over the hole to measure its absorption profile. The laser sweep is repeated several times and then the laser frequency is tuned off-resonance to 799 nm to determine the level for full transparency. Our result is shown by the dashed curve in Fig. 3. The width of the spectral hole is attributed to power broadening, laser jitter, and the resolution of the laser sweep (each of these contributions is verified by independent measurements). Although we have not yet quantified the effect of time-dependent spectral diffusion over 100 ms timescales under similar conditions, we believe that spectral diffusion does not play a role here as initial measurements have shown very little linewidth broadening over timescales up to  $\sim 1$  ms using a 300 G magnetic field and at a temperature of 800 mK, equivalent to that measured using a  $\text{Tm}^{3+}:\text{LiNbO}_3$  bulk crystal [19, 25].

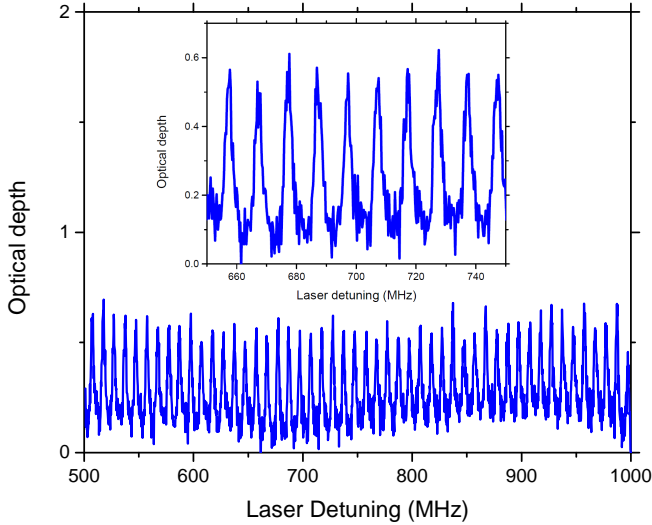


FIG. 4: A 0.5 GHz AFC prepared on a near-zero background. Inset: A 100 MHz-bandwidth section of the AFC shown in the main figure.

The variance in optical depth detuned from the hole is due to laser intensity modulation from optical cavities formed by waveguide and fiber endfaces. Next we increase the magnetic field to 2 kG and then perform the same hole burning sequence at different frequency detunings to create multiple spectral holes, each separated by 10 MHz from their neighbor. The result is a 100 MHz-bandwidth AFC programmed with a 100 ns storage time and finesse  $F$ , defined by the product of storage time and the linewidth of each tooth comprising the comb, of approximately two. Our AFC is shown by the solid curve in Fig. 3. Note that the 100 ms wait time is  $>30$  times greater than that used for storage of non-classical light [3], and chosen to demonstrate AFC persistence. The small optical depth of the comb is due to both the aforementioned laser-induced broadening and excitation during the read sequence. The residual background at the AFC edges is due to anti-holes, with some asymmetry induced by the interference effects. The antihole inhomogeneous broadening of  $\sim 50$  kHz/G at this wavelength [25] is consistent with that expected in a  $\text{Tm}^{3+}:\text{LiNbO}_3$  bulk crystal due to multiple Tm sites [19]. We expect the antiholes to narrow significantly at wavelengths closer to 794.3 nm [19].

To show that our waveguide is suitable for high data-rate applications employing AFCs beyond  $F = 2$ , we increase the field to 20 kG, and repeat the experiment, except now preparing a 0.5 GHz-bandwidth AFC programmed with 100 ns storage time and  $F = 3$ . The result is shown in Fig. 4. The short storage time, small optical depth, and small residual background is due to the same effects impacting the AFC shown in Fig. 3, except here we intentionally choose the AFC bandwidth

to be much smaller than the anti-hole splitting to have a vanishing absorption background at the AFC edges. Note that we have prepared and observed AFCs featuring a 2 GHz bandwidth and  $F \leq 10$  (going beyond our previous observation of  $F = 6$  [9]), however with very low optical depth (due to laser-induced broadening), and an antihole-induced background at the AFC edges. We expect that excitation at wavelengths closer to the center of the inhomogeneous line will allow AFC bandwidths of several GHz with vanishing absorption background using fields of tens of kilogauss.

Due to confinement of light, a waveguide light-matter interface generally allows for higher-frequency Rabi oscillations per photon than using a bulk optics arrangement. Thus, waveguides are desirable for both on- and off-resonant interaction, e.g. spectral tailoring, Raman interaction, or cross-phase modulation. To these ends, we quantify the magnitude of the  ${}^3\text{H}_6$  to  ${}^3\text{H}_4$  transition dipole moment  $\mu$  of our waveguide at a temperature of 800 mK under zero magnetic field using both optical nutation (at a wavelength of 795.3 nm) and two-pulse photon echo excitation (at a wavelength of 795.6 nm). The strength of the light-matter coupling is scaled by a ratio of  $\mu^2/A$  per photon, where  $A$  is the mode cross-sectional area. We note it is crucial that the magnitude of  $\mu$  be preserved after waveguide fabrication to obtain an advantage from a smaller  $A$ . We direct a pulse into the waveguide and, after interaction, detect a coherent modulation of the pulse intensity (i.e. nutation) – see Fig. 5a. We observe a time-dependent decay of the nutation indicating a distribution of Rabi frequencies due to transverse (Gaussian intensity distribution) and longitudinal (propagation loss) variation in the laser intensity as well as overlap of different atomic transitions (inhomogeneous broadening). The modulation is related to the effective Rabi frequency  $\Omega$ . We calculate an average  $\Omega$  using (i) the relative time between the beginning of the pulse and each discernible population inversion maxima and minima, and (ii) a scaling factor that depends on when the extrema occur [30]. By varying the input pulse power, we observe a linear  $\Omega^2$ -dependence. We plot our results in Fig. 5b and fit using,

$$\Omega^2 = \kappa \frac{\mu^2}{A} P, \quad (3)$$

where  $P$  is the estimated power in the waveguide,  $\kappa = 2(n^2 + 2)^2 / (9nc\epsilon_0\hbar^2)$  is a material constant [28],  $n$  is the index of refraction, and  $A \approx \pi (6.25 \mu\text{m})^2$  is estimated from independent beam-waist measurements. A fit of the curve reveals an average  $\bar{\mu} = (3.7 \pm 0.4) \times 10^{-32}$  C·m, agreeing well with the  $4 \times 10^{-32}$  C·m reported for a  $\text{Tm}^{3+}:\text{LiNbO}_3$  bulk crystal [19]. This dipole moment is one of the largest of all rare-earth-ion optical transitions that have been studied [23, 26].

To confirm our result, we perform a series of two-pulse echo excitation measurements where we restrict the sec-

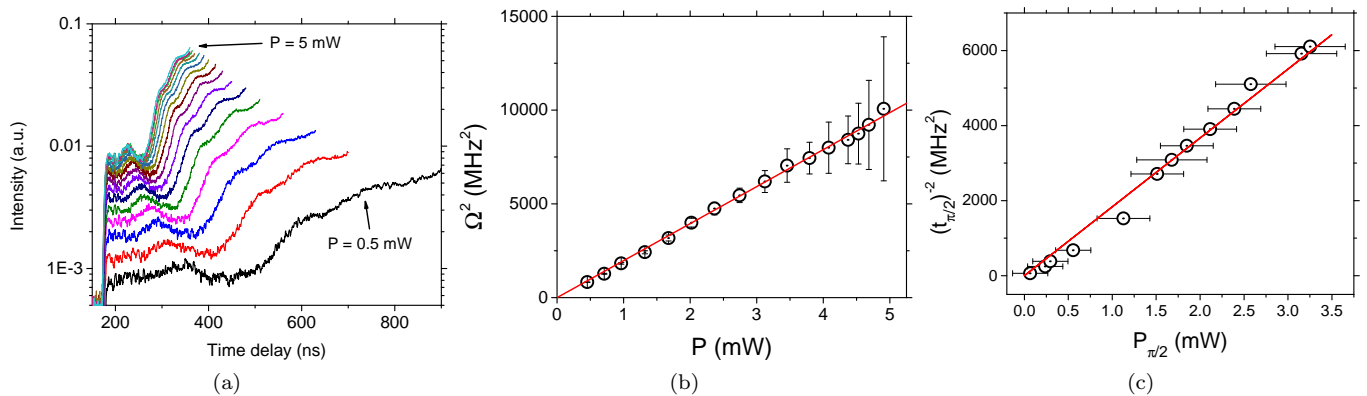


FIG. 5: Measurements of the transition dipole moment. (a) Observed optical nutation (log scale) using pulses of power  $P$  varied between 0.5 and 5 mW (shown with different colors). Curves are truncated to timescales where nutation is most visible. (b) Power dependence of  $\Omega^2$ . We calculate an average  $\Omega$  from each nutation using the first inversion maximum and minimum, and the second and third inversion maxima. (c) Pulse duration and power dependence from two-pulse photon echo experiments.

ond excitation pulse to have identical peak power  $P_{\pi/2}$  and twice the duration  $t_{\pi/2}$  of the first pulse. By increasing  $P_{\pi/2}$ , the condition of excitation using  $\pi/2$ - and  $\pi$ -pulses is found by observing a maximal echo intensity, and is repeated for varying  $P_{\pi/2}$  and  $t_{\pi/2}$ . Using the area theorem  $\pi/2 = \Omega t_{\pi/2}$  [28] and  $P \equiv P_{\pi/2}$ , we plot and fit our data to Eq. 3 (see Fig. 5c) giving  $\bar{\mu} = (7.3 \pm 0.1) \times 10^{-32}$  C·m, which is comparable to that extracted from our nutation measurements.

*Conclusion*—Using temperatures of only a few Kelvin less than those typically employed for optical quantum processing using rare-earth-ion-doped crystals [14, 15], we measure dramatically improved spectroscopic properties of  $\text{Tm}^{3+}:\text{Ti}^{4+}:\text{LiNbO}_3$  compared to previous work at 3 K [18], with performance surpassing other rare-earth-ion-doped waveguides [20–22], and properties of the ions within the Ti-modified host matrix matching those in the corresponding bulk  $\text{Tm}^{3+}:\text{LiNbO}_3$  crystal [19, 24]. Our results advance the development of low-loss quantum light-matter integrated circuits using industry-standard materials and shed light on the relationship between rare-earth-ion properties and crystal modification. However, more detailed investigation of other important properties of our waveguide, such as field-dependent spectral diffusion beyond 1 ms time delays and wavelength-dependent characteristics, are needed for optimal implementations and further understanding of any potential fabrication-induced modification of spectral properties due to either Ti-indiffusion or rare-earth doping.

We thank E. Saglamyurek and C. Deshmukh for discussions and help with early investigations, and M. George, R. Ricken, and W. Sohler for fabrication of the waveguide. We acknowledge funding through Alberta Innovates Technology Futures (AITF), the Natural Sciences and Engineering Research Council of Canada (NSERC), the US National Science Foundation (NSF)

under award nos. PHY-1415628 and CHE-1416454, and the Montana Research and Economic Development Initiative. Furthermore, W.T. acknowledges support as a Senior Fellow of the Canadian Institute for Advanced Research (CIFAR).

- 
- [1] W. Sohler, H. Hu, R. Ricken, V. Quiring, C. Vannahme, H. Herrmann, D. Büchter, S. Reza, W. Grundkötter, S. Orlov, H. Suche, R. Nouroozi, and Y. Min, *Opt. Photon. News* **19**, 24-31 (2008).
  - [2] M. Bazzan and C. Sada, *Appl. Phys. Rev.* **2**, 040603 (2015).
  - [3] E. Saglamyurek, N. Sinclair, J. Jin, J. A. Slater, D. Oblak, F. Bussi eres, M. George, R. Ricken, W. Sohler and W. Tittel, *Nature* **469**, 512-515 (2011).
  - [4] S. Tanzilli, A. Martin, F. Kaiser, M.P. De Micheli, O. Alibart, and D.B. Ostrowsky, *Laser & Photonics Rev.* **6**, 115143, (2012).
  - [5] E. Saglamyurek, N. Sinclair, J. A. Slater, K. Heshami, D. Oblak, and W. Tittel, *New J. of Physics* **16**, 065019 (2014).
  - [6] D. Bonneau, et al., *Phys. Rev. Lett.* **108**, 053601 (2012).
  - [7] J. Carolan, C. Harrold, C. Sparrow, E. Mart  n-L  pez, N. J. Russell, J. W. Silverstone, P. J. Shadbolt, N. Matsuda, M. Oguma, M. Itoh, G. D. Marshall, M. G. Thompson, J. C. F. Matthews, T. Hashimoto, J. L. O'Brien, and A. Laing, *Science* **349**, 711-716 (2015).
  - [8] T. Meany, M. Gr  fe, Ren   Heilmann, A. Perez-Leija, S. Gross, M.I.J. Steel, M. J. Withford, and A. Szameit *Laser & Photonics Rev.* **9**, 363384, (2015).
  - [9] N. Sinclair, E. Saglamyurek, H. Mallahzadeh, J. A. Slater, M. George, R. Ricken, M. P. Hedges, D. Oblak, C. Simon, W. Sohler, and W. Tittel, *Phys. Rev. Lett.* **113**, 053603 (2014).
  - [10] H. J. Kimble, *Nature* **453**, 1023-1030 (2008)
  - [11] N. Sangouard, C. Simon, H. de Riedmatten, and N. Gisin, *Rev. Mod. Phys.* **83**, 33 (2011).
  - [12] N. Sinclair, K. Heshami, C. Deshmukh, D. Oblak, C.

- Simon, and W. Tittel, arXiv:1510.01164 (2015).
- [13] M. P. Hedges, J.J. Longdell, Y. Li, and M. J. Sellars, *Nature* **465**, 1052 (2010).
  - [14] F. Bussi eres, N. Sangouard, M. Afzelius, H. de Riedmatten, C. Simon & W. Tittel, *J. Mod. Opt.* **60**, 18 (2013).
  - [15] H. de Riedmatten and M. Afzelius, in *Engineering the Atom-Photon Interaction Springer*, edited by Ana Predojevi  and Morgan Mitchell (Springer, 2015), Chap. 9.
  - [16] W. Tittel, M. Afzelius, T. Chaneli re, R. L. Cone, S. Kr  ll, S. A. Moiseev and M. Sellars, *Laser & Photonics Reviews* **4**, 244 - 267 (2010).
  - [17] M. U. Staudt, S. R. Hastings-Simon, M. Nilsson, M. Afzelius, V. Scarani, R. Ricken, H. Suche, W. Sohler, W. Tittel, and N. Gisin, *Phys. Rev. Lett.* **98**, 113601 (2007). M. U. Staudt, M. Afzelius, H. de Riedmatten, S. R. Hastings-Simon, C. Simon, R. Ricken, H. Suche, W. Sohler, and N. Gisin, *Phys. Rev. Lett.* **99**, 173602 (2007).
  - [18] N. Sinclair, E. Saglamyurek, M. George, R. Ricken, C. La Mela, W. Sohler, and W. Tittel, *J. Lumin.* **130**, 1586-1593 (2010).
  - [19] Y. Sun, C. W. Thiel, and R.L. Cone, *Phys. Rev. B* **85**, 165106 (2012). C.W. Thiel, Y. Sun, T. B  ttger, W.R. Babbitt, and R.L. Cone, *J. Lumin* **130**, 1598 (2010). C. W. Thiel, Y. Sun, R. M. Macfarlane, T. B  ttger, and R. L. Cone, *Journal of Physics B: Atomic, Molecular and Optical Physics* **45**, 12 (2012).
  - [20] S. Marzban, J. G. Bartholomew, S. Madden, K. Vu, and M. J. Sellars, *Phys. Rev. Lett.* **115**, 013601 (2015).
  - [21] T. Zhong, J. M. Kindem, E. Miyazono, and A. Faraon, *Nature Communications* **6**, 8206 (2015).
  - [22] G. Corrielli, A. Seri, M. Mazzera, R. Osellame, and H. de Riedmatten, arXiv:1512.09288 (2015).
  - [23] R. M. Macfarlane and R. M. Shelby, in *Spectroscopy of Solids Containing Rare Earth Ions*, edited by A. A. Kaplanskii and R. M. Macfarlane (North Holland, Amsterdam, 1987), Chap. 3.
  - [24] C. W. Thiel, N. Sinclair, E. Saglamyurek, D. Oblak, W. Tittel, and R. L. Cone (unpublished).
  - [25] N. Sinclair, E. Saglamyurek, D. Oblak, C. W. Thiel, R. L. Cone, and W. Tittel (unpublished).
  - [26] D. L. McAuslan, J. J. Longdell, and M. J. Sellars, *Phys. Rev. A* **80**, 062307 (2009).
  - [27] F. Marsili, V. B. Verma, J. A. Stern, S. Harrington, A. E. Lita, T. Gerrits, I. Vayshenker, B. Baek, M. D. Shaw, R. P. Mirin, and S. W. Nam. *Nature Photon.* **7**, 210214 (2013).
  - [28] C. W. Thiel, R. M. Macfarlane, Y. Sun, T. B  ttger, N. Sinclair, W. Tittel and R. L. Cone, *Laser Physics* **24**, 106002 (2014).
  - [29] W. B. Mims, *Phys. Rev.* **168**, 370 (1968).
  - [30] Y. Sun, G. M. Wang, R. L. Cone, R. W. Equall, and M. J. M. Leask, *Phys. Rev. B* **62**, 15443 (2000). A. Louchet, J. S. Habib, V. Crozatier, I. Lorg  r  , F. Goldfarb, F. Bretenaker, J.-L. Le Gou  t, O. Guillot-No  l, and P. Goldner, *Phys. Rev. B* **75**, 035131 (2007).